Bioactive Materials 3 (2018) 39–47

Contents lists available at ScienceDirect

Bioactive Materials

journal homepage: http://www.keaipublishing.com/en/journals/bioactive-materials/

Highly photostable nanogels for fluorescence-based theranostics

Dipendra Gyawali [a], Jimin P. Kim [b], Jian Yang [b, *]

[a] Department of Bioengineering, The University of Texas at Arlington, Arlington, TX 76010, USA
[b] Department of Biomedical Engineering, Materials Research Institute, The Huck Institutes of The Life Sciences, The Pennsylvania State University, University Park, PA 16802, USA

ARTICLE INFO

Article history:
Received 2 February 2017
Accepted 6 March 2017
Available online 27 March 2017

Keywords:
Nanogels
Fluorescent polymer
Drug delivery
Cellular imaging
Bioconjugation

ABSTRACT

A novel photo-crosslinkable nanogel is prepared from a biodegradable polymer template with intrinsic photoluminescence and high photostability. The fluorescent nanogels display excellent biodegradability and cytocompatibility owed to the facile synthesis scheme involving a solvent- and surfactant-free one-pot reaction, derived entirely from biocompatible monomers citric acid, maleic acid, L-cysteine, and poly(ethylene glycol). The resultant nanogels are less than 200 nm in diameter with a narrow size distribution and monodispersity, and demonstrate long-term structural stability in biological buffer for two weeks. To gauge potential in theranostic applications, the fluorescent nanogels were surface functionalized with biologically active RGD peptides and encapsulated with active anti-cancer drug Doxorubicin, resulting in a pH-responsive controlled drug release in acidic pH resembling tumor environments. The strong fluorescence of the nanogels enabled tracking of targeted drug delivery, showing that drug-loaded nanogels homed into the cytoplasmic regions of prostate cancer cells to significantly induce cell death. These photo-crosslinkable and biodegradable nanogels pose as a strong candidate for theranostic medicine, demonstrating versatile functionalization, high stability in biological buffers, and capacity for real-time fluorescence-based monitoring of targeted drug delivery.

1. Introduction

The advance of biodegradable nanoparticles with increasingly sophisticated functions has made far-reaching impact in biomedical engineering to expand bioimaging and drug delivery systems [1–3]. Among these, soft (hydrogel-based) crosslinked nanoparticles offer unique advantages over other drug delivery systems, such as enhanced in-vivo stability, complex interior networks to incorporate bioactive molecules, tunable size ranging from several micrometers to tens of nanometers, and large surface areas for biofunctionalization [4–6]. Furthermore, the use of synthetic polymers in the preparation of crosslinked soft nanoparticles can provide additional advantages in controlling physical, chemical, and biological properties by tailoring the polymer chain and functionality, while accommodating a wider range of monomers with desirable chemistry [7–9].

Recently the diagnostics and therapeutics of disease such as cancer has evolved remarkably due to the rise of multi-functional soft nanoparticles, enabling imaging within delivery systems [10–14]. Fluorescence-based bioimaging offers particular advantages such as high sensitivity and rapid response kinetics [6]. Among fluorescent probes, organic dyes [15] and quantum dots [16–18] are the most widely used that can be encapsulated within or conjugated to the nanoparticle system. However, organic dyes suffer from rapid photobleaching and poor photochemical stability whereas heavy metals (cadmium and selenide) in quantum dots are toxic to living organisms. Moreover, encapsulation or conjugation of fluorescence probes within nanoparticle systems leads to poor performance issues due to leaching, inhomogeneity, or degradation of the fluorescent moieties. As such, materials with intrinsic fluorescence would have a momentous advantages in terms of simplicity and reliability of bioimaging modalities. Much effort in recent years have been directed towards development of intrinsically fluorescent nanoparticles, leading to innovative materials such as carbon nanoparticles [19], silica nanoparticles [20], and intrinsically fluorescent polymeric nanoparticles [21].

Our research group has had a long-standing interest in the development of such intrinsically fluorescent nanoparticles that

* Corresponding author.
E-mail address: jxy30@psu.edu (J. Yang).
Peer review under responsibility of KeAi Communications Co., Ltd.

http://dx.doi.org/10.1016/j.bioactmat.2017.03.001

can be prepared from biodegradable polymers. Recently, we synthesized biodegradable photoluminescent polymers (BPLPs) that can emit strong fluorescence with high quantum yield and strong photostability [22]. These polymers demonstrated significant biomedical value in their capacity for fluorescence-based bioimaging, implantable devices such as tissue engineering scaffolds [23], and drug delivery nanoparticles [24–26]. More importantly, the facile synthesis scheme involved a simple polycondensation reaction between metabolites such as citric acid, an amino acid and a diol without the use of solvents or catalysts, facilitating the development of biologically compatible materials. Although BPLPs can precipitate into nanoparticles in water-organic solvent interfaces, they tends to aggregate due to the low molecular weight of BPLPs, severely limiting their potential as theranostic probes. Herein, we describe a simple and convenient strategy for the preparation of highly photostable crosslinked hydrogel particles (nanogels) based on the BPLP template, derived entirely from biocompatible monomers such as citric acid and maleic acid (metabolites in the Krebs cycle) and L-cysteine (an essential amino acid), as well as poly(ethylene glycol) (PEG, widely used in FDA-approved biomaterials). We first synthesized water soluble BPLPs with free radical linkable double bonds to generate photocrosslinkable biodegradable photoluminescent polymers (PBPLPs). These low molecular weight fluorescent polymer chains were crosslinked into nano-scale hydrogels (nanogels) in the presence of a photoinitiator when exposed to ultra violet (UV) light for a few minutes in an aqueous system. The resultant nanogels exhibited strong photoluminescent properties, excellent biocompatibility and detectable cell labeling. Moreover, surface rich functional groups of these nanogels enabled conjugation of a variety of biologically active molecules. These nanogels can be prepared in biologically relevant buffers and media with excellent stability, while demonstrating complete degradation within two weeks. Anticancer drug (DOX) was also incorporated within these fluorescent nanogels to demonstrate efficacy in tracking intracellular drug delivery.

2. Results and discussion

Our synthetic strategy is unique in that overall toxicity inherited by the prepared polymers and nanogels is made minimal by: (1) careful selection of biocompatible monomers, (2) mild one-pot reaction conditions, and (3) avoidance of organic solvents and toxic catalysts. PBPLP polymers are synthesized by a simple polycondensation reaction between carboxylic groups (from citric acid or maleic acid), amine groups (L-cysteine used herein), and a diol (from PEG) to create a low molecular weight polymer chain containing degradable ester and amide bonds, along with an olefin group susceptible to free radical crosslinking (Fig. 1).

The weighted-average molecular mass as measured by MALDI-MS was found to be 1026 Da with a polydispersity index of 1.21 (Fig. S1). NMR chemical shifts featured CH=CH− groups at 6.4 and 6.8 (a), CH2- at 2.9 (b), 3.5 (c), and 4.2 (d) supporting the formation of the proposed structure in Supplementary Fig. S2. After integrating the area under Peak A (characteristic peak for maleic acid), B (characteristic for citric acid), and D (characteristic for ester bond linked PEG), we further confirmed that the ratio between these monomers (0.47:0.51:0.95) within the polymer chains closely matched the feeding ratio (0.5:0.5:1.0) of the monomers citric acid, maleic acid and PEG respectively. It should be noted that the upfield shift of peak B from 2.68 (as in pure citric acid) to 2.9, formation of a new peak at 6.8 (a) compared to pure maleic acid and formation of new peak at 4.2 (d) as compared to pure PEG molecules further supported that polycondensation occurred between carboxylic acid and hydroxyl groups to create PBPLP polymer chains.

To prepare PBPLP nanogels, we dissolved low molecular weight PBPLP polymers in water with low molar ratios of acrylic acid (as crosslinker) and AMPAD (as photo initiator), subjecting them to 395 nm UV light for 15 min, while once again avoiding the use of toxic surfactants and solvents (Scheme 1). The formulated nanogels possessed an average hydrodynamic diameter of 119 ± 47 nm with a mode of 78 nm, with 90% of the nanogels within 185 nm without any evidence of aggregation even at higher concentrations (14.97 × 108 particles/ml) according to the nanogel distribution graph (Fig. 2A). TEM micrographs of PBPLP nanogels revealed spherical particles with good monodispersity (Fig. 2B).

Next, we suspended the nanogels in 0.1 M PBS (pH 7.4) for two weeks to study long-term stability. The nanogels were highly stable during the two weeks, well-maintaining structural integrity with a hydrodynamic diameter within 150 nm (Fig. 2C), after no

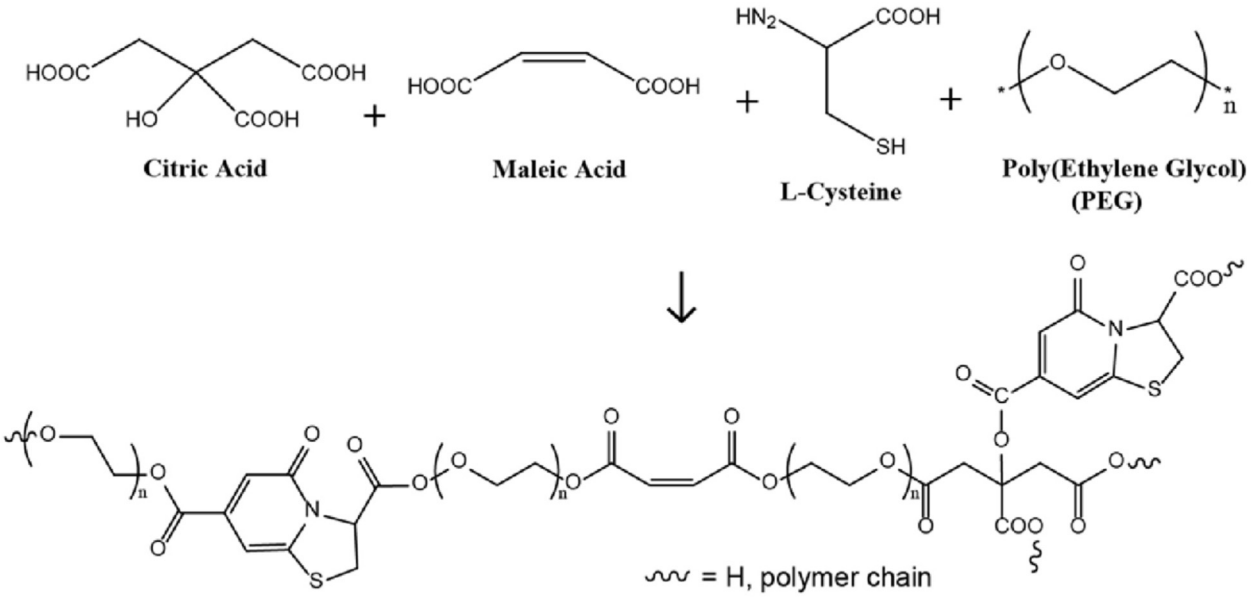

Fig. 1. Monomers used in the synthesis of PBPLP polymer.

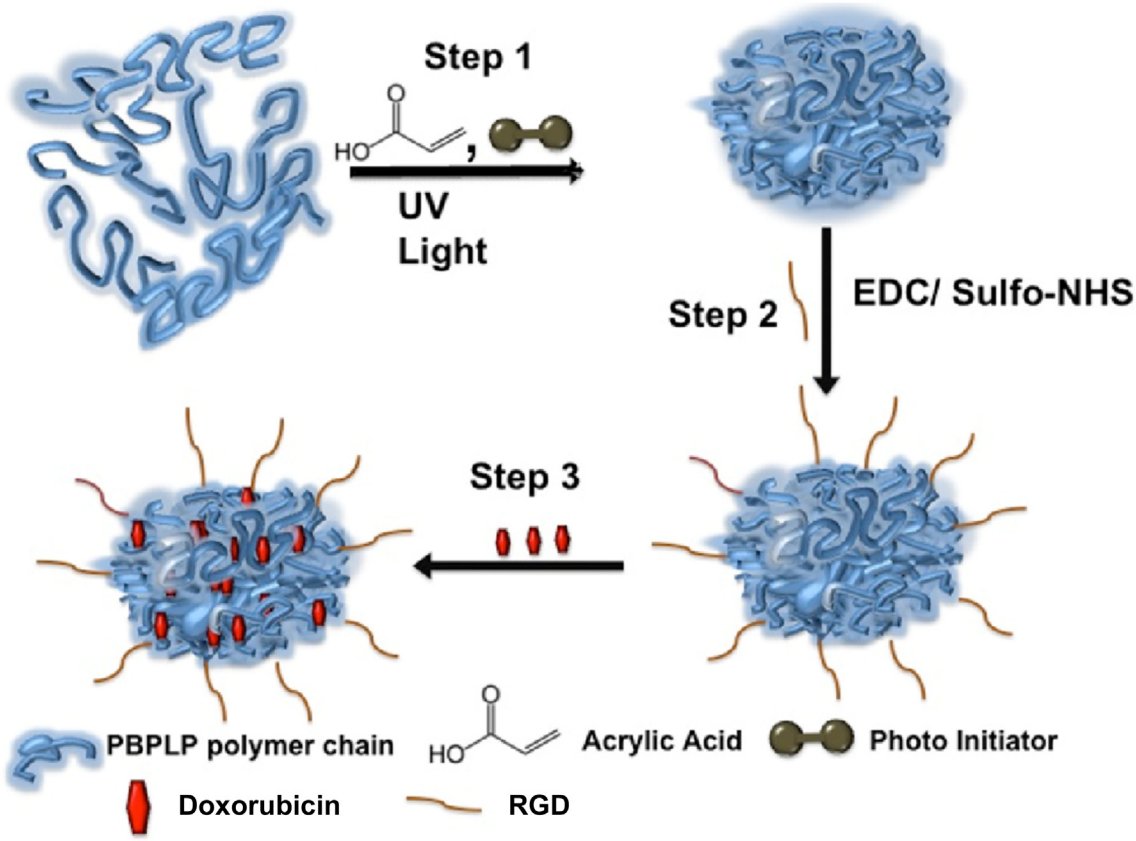

Scheme 1. Schematics of RGD functionalized, DOX loaded, fluorescence emitting crosslinked PBPLP nanogels. (Step 1) Photocrosslinkable fluorescent polymer (PBPLP) crosslinked into fluorescent nanogels in the presence of a photo-initiator, acrylic acid, and UV light; (Step 2) PBPLP nanogels can be surface functionalized with biologically active molecules (herein, RGD peptide) using EDC/sulfo-NHS chemistry; (Step 3) Doxorubicin (anti-cancer drug) can be encapsulated within these soft particles to create surface functionalized, fluorescence emitting drug delivery vehicles.

detectable size of the nanoparticles were observed. They continuously maintained structural integrity for 15 days and completely degraded with no detectable size. As long-term stability in buffer is essential for bio-applications, we further interrogate studied the nanogel stability in PBS at 37° C at low concentrations (0.5 mg/ml) and high concentrations (5 mg/ml) and observed under NanoSight LM10 equipped with an optical microscope. As seen in movie S1 and S2, PBPLP particles are were highly stable in either concentration without noticeable aggregation (Supporting Information). Following, we studied the surface charge of PBPLP nanogels, revealing a surplus of anionic moieties with zeta potential value of −25, which suggested potential for conjugating bioactive molecules or enabling pH-sensitive applications (Fig. 2D).

Supplementary video related to this article can be found at http://dx.doi.org/10.1016/j.bioactmat.2017.03.001.

To gauge potential in theranostic applications, we subsequently investigated the fluorescence properties of our PBPLP polymers and nanogels that may enable fluorescence-based tracking of drug delivery. Remarkably, PBPLP polymers exhibited a strong maximal emission of 443 nm under 370 nm excitation (Fig. 3A), even maintaining strong fluorescence following fabrication into nanogels (Fig. 3B). The quantum yield of the nanogels were measured to be 11% (Fig. 3C), higher than traditional fluorescent labels such as fluorescent polymer N-Gal HPAMAM (7.9%), blue fluorescent protein (7.9%), green fluorescent protein (7.3%), and Cy3 dye (3–5%). In our previous systematic investigation of the fluorescence mechanism of biodegradable photoluminescent polymers (BPLPs), we reported that BPLPs could be synthesized with any of the 20 essential amino acids to develop a versatile family of fluorescent polymers with bright tunable fluorescence, high quantum yield, and strong photostability compared to traditional organic fluorescent labels, along with various chemical sensing functions [27,28]. The work herein focused on PBPLPs derived from L-cysteine, given that the resultant polymer exhibited particularly high fluorescence properties such that PBPLP nanogels could be well observed under DAPI filter in cytoviva microscopy as mono-dispersed blue dots (Fig. 3D).

Next, bio-functionalization of PBPLP nanogels is provided by the use of acrylic acid as a crosslinker (Scheme 1), in which its vinyl groups acid participate in free radical crosslinking of the polymer chain while its pendant carboxyl groups serve as an ideal site to conjugate various biomolecules via amino groups. Here we demonstrated this functionalization by conjugating cyclic RGD peptide, which are known to target cells expressing avβ3 integrins such as in tumor vasculature. Conjugation of RGD by EDC/NHS chemistry was verified at each step by FTIR. Initially, the spectra of PBPLP nanogels presented a sharp peak at 1710 cm−1 corresponding to the carboxyl group, a weak shoulder at 1640 cm−1 for the vinyl group, a broad peak at 3400 cm−1 for the hydroxyl group and a peak at 2850 cm−1 for the alkane group (Fig. S3). Upon successful activation with EDC/NHS, multiple weak shoulders appeared beside the primary carboxyl peak, along with a C–N stretch at 1360 cm−1 and a sulfoxide group at 1050 cm−1 (from the sulfo-NHS). Lastly, upon conjugation with RGD, FTIR revealed relatively intense amide bands at 1634 and 1542 cm−1, while the relative intensity of the carboxyl peak at 1710 cm−1 diminished and the sulfoxide peaks at 1050 cm−1 disappeared. A broad band at 3200 cm−1 also emerged, indicating the presence of amine groups.

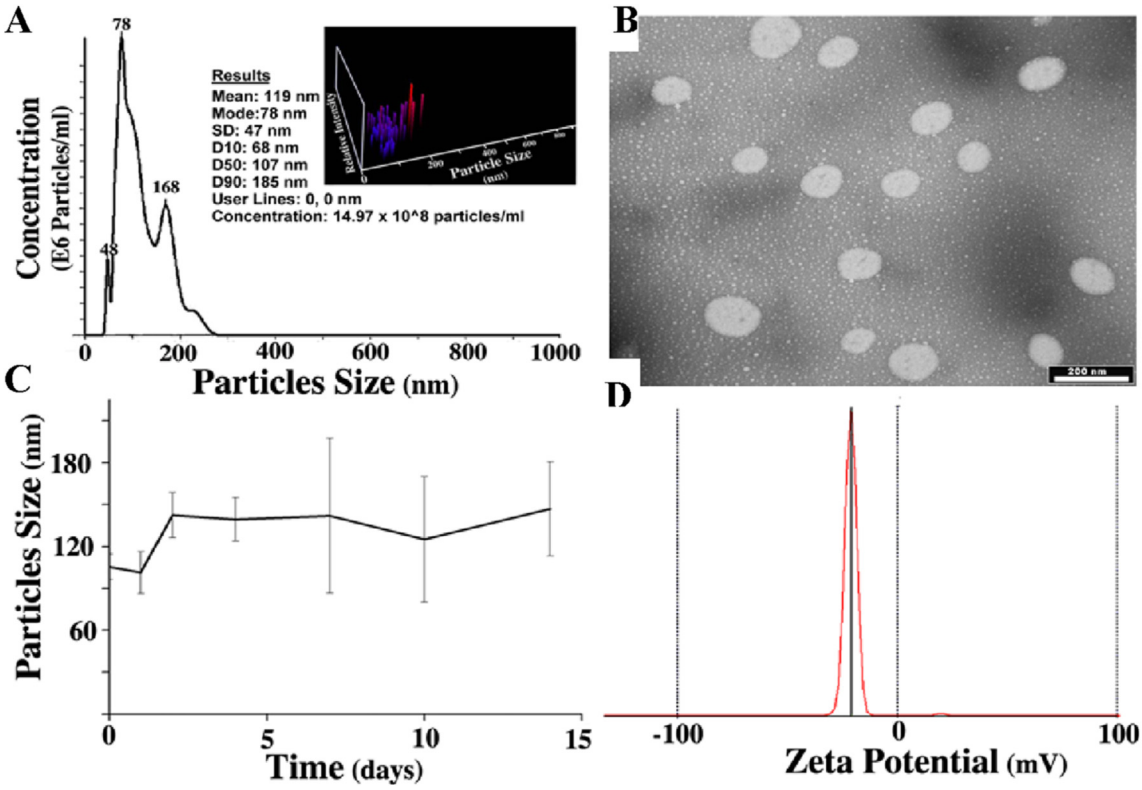

Fig. 2. A) Particle size distribution of PBPLP nanogels recorded by Nanosight LM20, spectrum in the inset represents the 3D plot of particle population resolved in terms of relative intensity and particle concentration. B) micrograph of nanogel morphology observed under TEM (scale bar = 200 nm), C) Nanogel size stability evaluation in PBS (pH 7.4) for a two week time period, and D) Zeta potential evaluated by a zeta potential analyzer.

Upon successful conjugation of RGD peptide, we subsequently evaluated the cellular toxicity of RGD-conjugated PBPLP nanogels at various concentrations (1, 10, 100, and 1000 μg/ml) and at fixed time periods (1, 2, and 3 days) against PC3 cells. PBPLP nanogels exhibited excellent cytocompatibility even at high concentrations, with dosages up to 1 mg/ml showing cell viability over 90% (normalized to that of free medium) upon 72 h incubation (Fig. 4A). Fluorescence microscopy confirmed the cellular uptake of nanogels with little morphological change in PC3 cells, showing promise in biological labeling applications (Fig. 4B). Interestingly, the intracellular accumulation of fluorescence signals indicated that RGD-conjugated PBPLP nanoparticles homed into the cytoplasmic regions (Fig. 4C), likely mediated by the avβ3 integrins presented on the prostate cancer cells.

Following this demonstration of RGD-mediated tumor targeting, the last step in realizing therapeutic delivery systems is the encapsulation of anti-cancer agents. Anti-cancer drugs, although highly potent, typically suffer from low water solubility that severely limit their efficacy in tumor-targeted treatments. Here we demonstrate that PBPLP nanogels loaded with doxorubicin (DOX) enable effective anti-cancer drug delivery, given the favorable hydrophilicity of the nanoparticles and the intricate polymeric networks that enhance drug loading capacity. RGD-conjugated PBPLP nanogels, when loaded with 20 wt% of DOX, displayed water solubility up to 50 mg/mL and encapsulation efficiency as high as 92%, indicating a significant improvement in DOX solubilization upon encapsulation into the hydrophilic nanogels. We postulate that the abundance of pendant carboxyl groups within the polymeric nanogel network may grant such high drug retention, further stabilizing the cationic drug by ionic interaction. Encapsulating DOX within PBPLP nanogels resulted in only a slight increase in the average nanoparticle diameter (129 ± 40 nm) (Fig. 5A).

We explored additional strategies for targeted drug delivery, such as pH-responsive controlled release. Such pH-sensitive systems are invaluable for the delivery of drugs to specific organs or cellular compartments, such as to the acidic environments of the stomach (pH 1.2) or lysosomes (pH 4.5), as well as to the slightly acidic (pH 6.5) microenvironments of tumors. Other studies of carboxylic acid-containing polymer systems have reported higher release rates of doxorubicin at pH 5 compared to those of pH 7.4, likely due to the electrostatic barrier induced by the ionizable carboxyl groups to alter the kinetics of retention and release in cationic drugs [29]. Our release studies of DOX revealed that a slightly acidic environment (pH 5.2) significantly enhanced the release rate of our nanogels compared to that of physiological pH (Fig. 5B). Although the initial burst release (21% within 3 h) was identical at either pH, the final release of DOX at pH 5.2 was 95% after 70 h compared to only 57% release at pH 7.4. The DOX-loaded RGD-PBPLP nanogels demonstrated steady and controlled release of DOX over the 70 h period, with a nearly doubled release rate in slightly acidic conditions, showing promise in pH-responsive drug delivery.

Lastly, we evaluated the pharmacological efficacy of the DOX-loaded RGD-PBPLP nanogels against PC3 cells by monitoring time and dose dependent toxicity with the MTT assay (Fig. 5C). We chose three nanogels concentrations (5, 25, and 50 μg/mL) each loaded with 20 wt% of DOX, normalizing viability with respect to a pure media control. Only DOX-loaded nanogels at 50 μg/mL showed significant toxicity by 24 h, reaching a critical reduction (>80%) in viability by 48 h on par with that of the positive control (10 μg/mL of free doxorubicin). Light microscopy of cell morphology

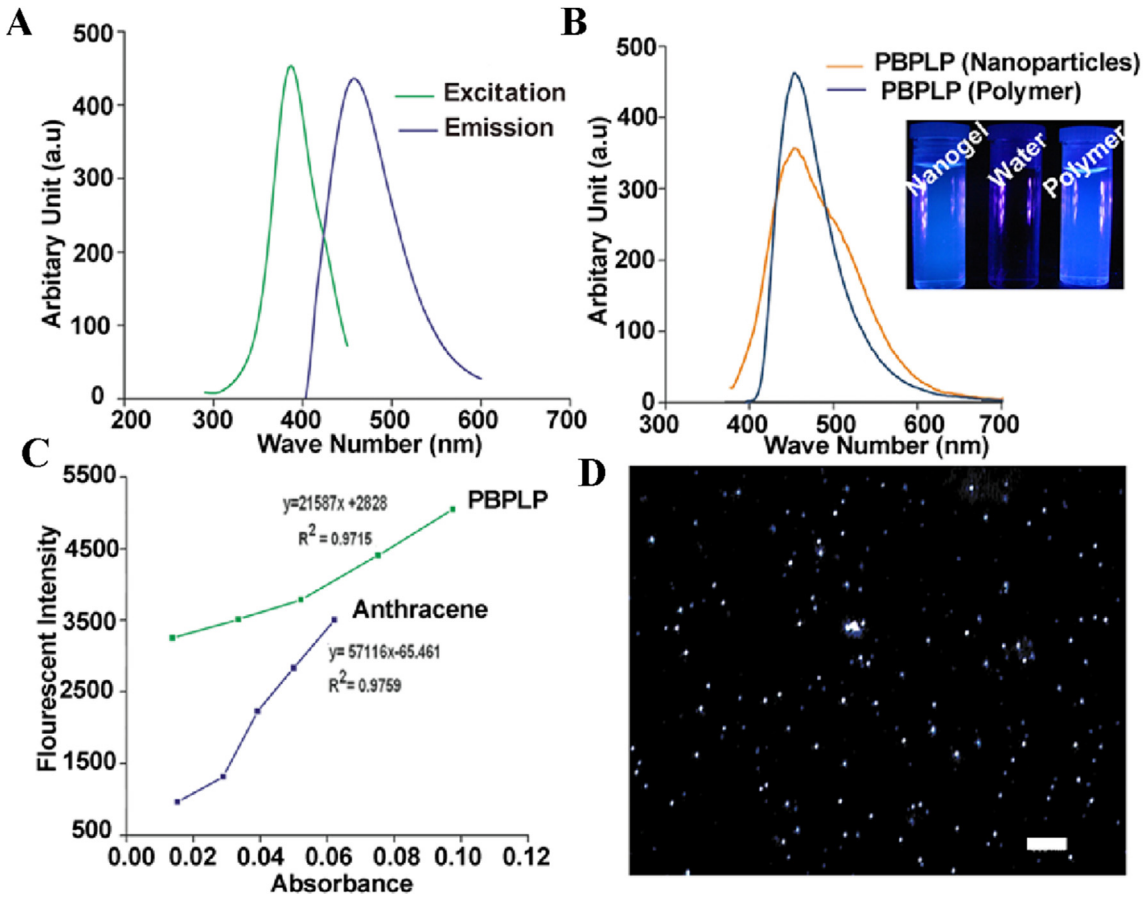

Fig. 3. A) Excitation and emission spectra of PBPLP polymer in water, B) Emission spectra of PBPLP polymer and nanogels in solution, C) Intensity-absorbance curve of PBPLP nanogels for quantum yield measurement, and D) Fluorescent micrograph of PBPLP nanogels obtained by cytoviva (scale bar = 500 nm).

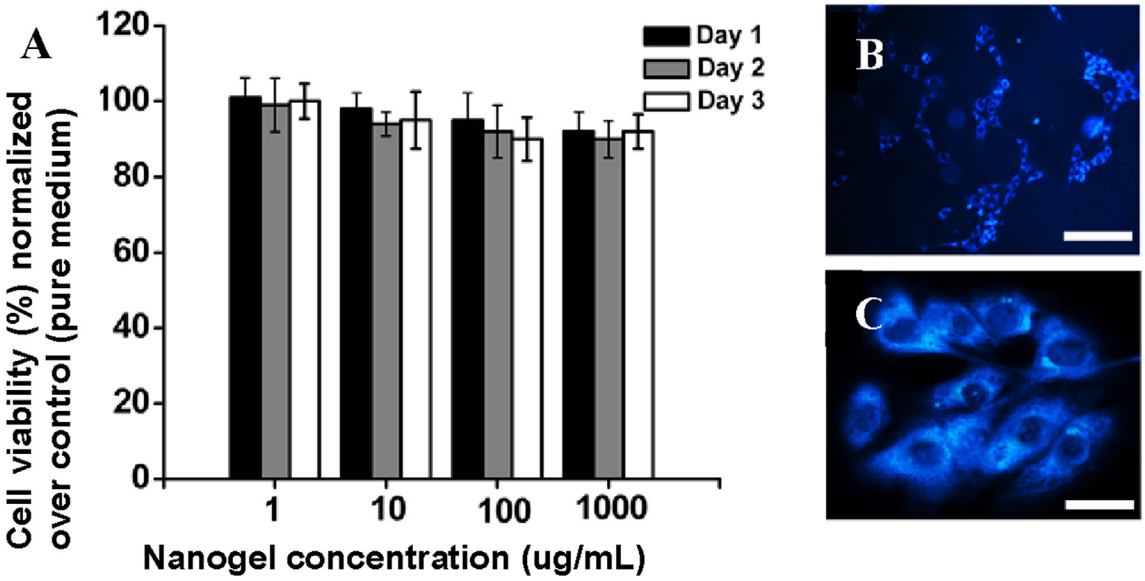

Fig. 4. A) Cytocompatibility of PBPLP nanogels against PC3 cells, B-C) Fluorescent micrograph of PC3 cells labeled with PBPLP nanogel after 8 h of incubation at 1000 μg/ml at 5× (B) and 20× magnification (C).

confirmed that pharmacological activity was evident by 24 h, with highly swollen cell nuclei and reduced cytoplasmic regions (Fig. 5D). Pure PBPLP nanogels showed no sign of cellular toxicity, suggesting that pharmacological activity only operates by controlled release of DOX compounds. We confirmed the intracellular delivery of DOX via PBPLP nanogels by fluorescence

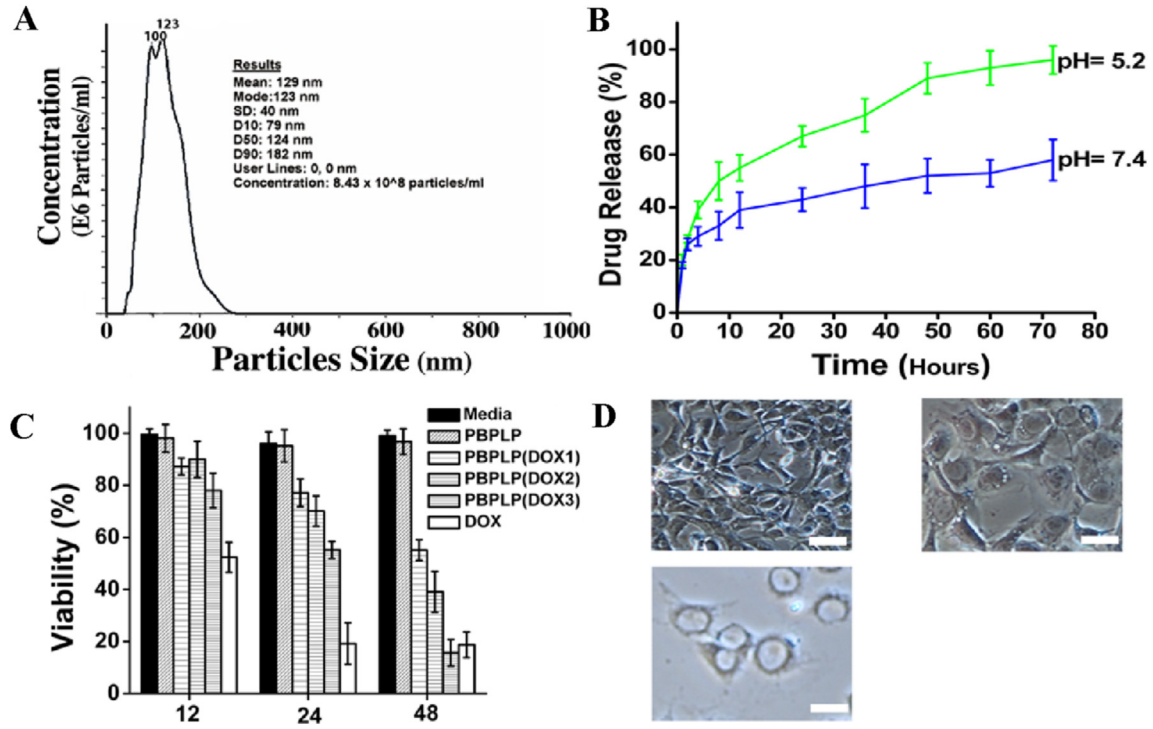

Fig. 5. A) Particle size distribution of PBPLP nanogels. B) Drug release profiles of PBPLP/DOX nanogels in 0.1 M acetic acid (pH 5.2) and 0.1 M phosphate buffer (pH 7.4). C) Pharmacological activity of PBPLP/DOX against prostate cancer cell lines (PC3). Figure legend: Media = pure media (negative control); PBPLP = 50 μg/ml nanogel (DOX-free control); PBPLP(DOX1, 2, or 3) = 5, 25, or 50 μg/ml respectively of nanogel loaded with 20 wt% of DOX; DOX = 10 μg/ml DOX (positive control). D) Light microscopy of PC3 cells incubated with PBPLP/DOX3 at 12 h (top left), 24 h (right), and 48 h (bottom left).

microscopy (Fig. 6). Intense blue fluorescence emitted by our nanogels internalized within the cytoplasmic regions of cells, whereas red fluorescence emitted by free or released doxorubicin accumulated within the cellular nuclei via DNA intercalation, suggesting that the release of DOX from PBPLP nanogels occurred predominantly after intracellular internalization.

3. Conclusions

In conclusion, we have developed bio-functionalized nanogels with intrinsic fluorescence. The synthesis strategy utilizes biocompatible molecules while avoiding expensive equipment, harsh reaction conditions, and complex schemes. Significantly,

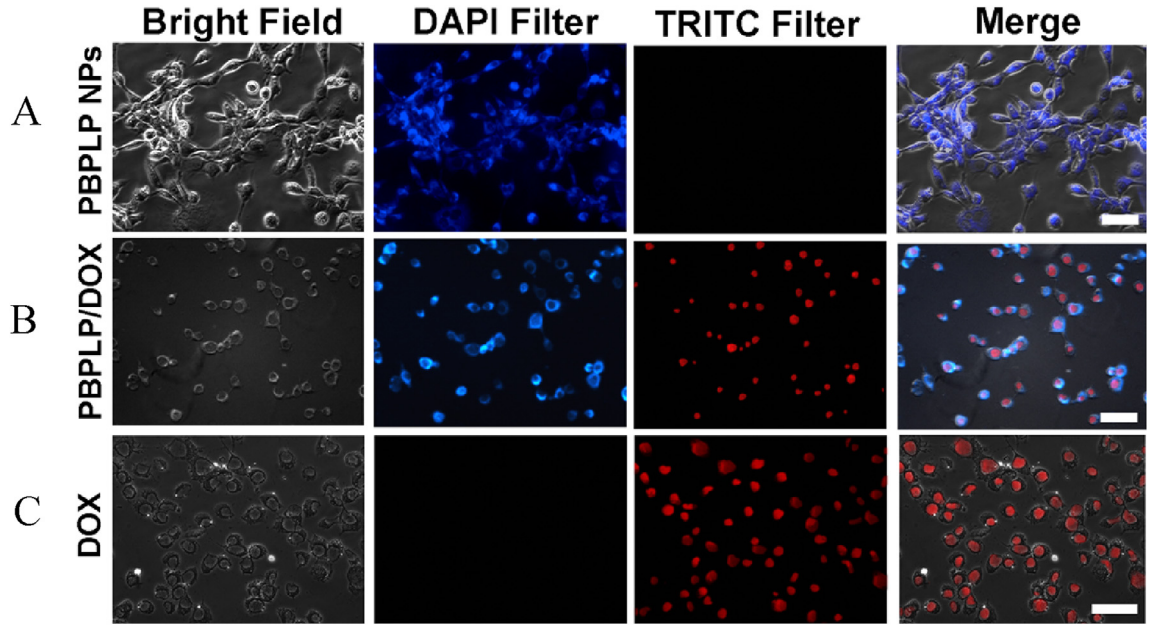

Fig. 6. Cellular internalization of PBPLP/DOX and delivery of DOX to the nucleus. Bright field and fluorescent micrograph of cellular uptake for (A) PBPLP nanogels, (B) PBPLP/DOX (50 μg/ml), and (C) free DOX (1 μg/ml) at 24 h. PBPLP nanogels stain the cytoplasm and free or released DOX stains cell nuclei. Scale bar 50 μm.

PBPLP nanogels feature excellent stability in biological media, strong photoluminescent properties, pH sensitive drug release, favorable biocompatibility and noticeable intracellular distribution. As a result, PBPLP nanogels may serve as a potential candidate for theranostic drug delivery, with the capacity to simultaneously identify tumor regions and deliver anti-cancer drugs to tumor sites in response to changes in pH.

4. Experimental section

4.1. Materials and instrumentation

All chemicals were purchased from Sigma-Aldrich and used without additional purification. All solutions were prepared using Milli-Q water (Millipore) as the solvent. The weighted average molecular weights of the polymer chains were analyzed using an Autoflex matrix-assisted laser desorption/ionization mass spectroscope (MALDI-MS; Bruker Daltonics). 2-(4-Hydroxyphenylazo)-benzoic acid (HABA) was used as the matrix to mix with the PBPLP in a 1:1000 pre-polymer/matrix molar ratio. The peaks from the main distribution and all sub-distributions were taken in consideration in the calculation of the weighted-average molecular mass of the polymers. Fourier Transform Infrared (FTIR) spectroscopy measurements were recorded at room temperature using a Nicolet 6700 FTIR (Thermo Scientific, Waltham, MA) equipped with OMNIC Software. 128 scans across the wave numbers 4000-500 cm_1 at a resolution of 2 cm_1 were taken to analyze bond vibration of functional groups associated with the molecular structure. Proton Nuclear Magnetic Resonance (1H NMR) was measured on 300 MHz JNMECS 300 (JEOL, Tokyo, Japan). The chemical shifts for the 1H NMR spectra were recorded in parts per million (ppm), and were referenced relative to tetramethylsilane (TMS, 0.00 ppm) as the internal reference. For chemical shift of various protons associated with the proposed structures, the purified polymer was dissolved in dimethyl sulfoxide-d6 (DMSO-d6) and placed in a 5 mm-outer diameter tube. Nanogels were prepared in a beaker placed into a sonicator water bath and subjected to a UVP 365 nm long-wave (ca. 4 mW/cm2, model 100AP, Blak-Ray). Sizes of the nanogels were evaluated by NanoSight LM20 (Nanosight Ltd., Amesbury, United Kingdom) equipped with an optical microscope and video camera. Nanogel solutions were injected into the sample chamber and a video of typically 60 s durations were taken (30 frames per second) and particles movements were analyzed by NTA software (Nanosight Ltd.) by tracking their Brownian movement. The velocity of particle movements were used to calculate particle sizes by applying the two-dimensional Stokes-Einstein equation. NTA post-acquisition settings were optimized and kept constant to analyzed the mean, mode, median, and concentration of the nanogels in the solution. Particle morphology was observed under transmission electron microscopy (TEM, JEOL 1200 EX, Tokyo, Japan). TEM was operated at an acceleration voltage of 80 kV. Samples for TEM observation were prepared by depositing a drop of nanogel solution onto a mesh copper grid coated with carbon. After the deposition, the aqueous solution was blotted away with a strip of filter paper and allowed to dry spontaneously. Surface charge of the nanoparticles was obtained using zeta potential analyzer with a DLS detector (ZetaPALS, Brookhaven Instruments, NY). Photoluminescence spectra of PBPLP pre-polymer and nanogel solutions were acquired on a Shimadzu RF-5301 PC spectrophotometer. All samples were set to concentrations of 3% (w/v). Both the excitation and the emission slit widths were set at 1.5 nm for all samples unless otherwise stated. The relative cytotoxic effects of the nanogels were evaluated using MTT colorimetric assays (CellTiter 96® AQueous One Solution Cell Proliferation Assay, Promega Corp., Madison, WI)) against Prostrate cancer cells line (PC3). The absorbance of the tetrazolium salt solution was measured at 570 nm using with an Infinite200 microplate reader (Teacan Group Ltd., Switzerland). To evaluate cellular uptake, cells were observed under a Leica DMLP microscope (Nikon).

4.2. Synthesis of PBPLP polymer

Photocrosslinkable Biodegradable Photoluminescent Polymer (PBPLP) polymer was synthesized by polycondensation reaction in nitrogen atmosphere. Briefly, 9.5 gm of citric acid, 20.1 gm of polyethylene glycol (Mw = 200 Da), and 6 gm of maleic acid were melted in a 250 mL three necked round bottom flask fitted with an inlet adapter and outlet adapter by stirring the contents in the flask at a temperature of 160 °C for 30 min. Once the constituents melted, 2 gm of L-cysteine were added to the reaction flask. Following this, the temperature was reduced to 140 °C and the pressure was reduced to 50 mTorr. The reaction was continued until the desired viscosity was achieved. The polymer was dissolved in deionized (DI) water and dialyzed (500 Da molecular-weight-cutoff membrane) for 2 days followed by lyophilization to achieve a purified form of the polymer of PBPLP. The purified BPLP polymer was further characterized for molecular weight, chemical shift of various protons associated with the proposed structure, characteristic bond vibrations of respective functional groups present in PBPLP polymer and photoluminescent properties.

4.3. Preparation of PBPLP nanogels

PBPLP nanoparticles were synthesized by free radical crosslinking initiated by a photoinitiator under 365 nm light. The nanoparticle fabrication procedure is as follows: 0.25 g of PBPLP polymer, 50 μL of acrylic acid, and 0.01 g of (2,2′-Azobis(2-methylpropion amidine)dihydrochloride) (AMPAD) were dissolved in 50 ml of deionized (DI) water. The solution was sonicated for one cycle lasting about 15 min followed by another cycle under exposure to 365 nm wavelength radiation. Solution was observed to turn cloudy, confirming the production of nanogels. Following this, the nanogel solution was centrifuged at 25,000 rpm for 20 min at room temperature. The retrieved nanoparticle pellets were resuspended at a concentration of 1% (w/v) in fresh DI water for further characterization. Nanogel size distributions were evaluated using NanoSight LM20 (Nanosight Ltd., Amesbury, United Kingdom) equipped with an optical microscope and a video camera. The colloidal stability of PBPLP nanoparticles was evaluated by suspending the nanoparticles in the commonly used biological buffer, Dulbecco's phosphate-buffered saline (PBS, pH 7.4). Nanogels were incubated in 0.1 M PBS at 37 °C for 3 weeks and particle sizes were measured at predetermined time points. General morphology of the particles was observed under TEM (JEOL 1200 EX, Tokyo, Japan). The fluorescent quantum yield of the nanogels was measured according the Williams method. The nanogels were dispersed in water and scanned at the optimal excitation wavelength. Nanogel solutions with different concentrations were measured and the graphs of integrated fluorescence intensity vs. absorbance were plotted. The quantum yields of the ABPLPs were calculated according to Equation (1)

$$\Phi X = \Phi ST \frac{SlopeX}{SlopeST}\left(\frac{\eta X}{\eta ST}\right)^2 \quad (1)$$

where, Φ = quantum yield; Slope = gradient of the curve obtained from the plot of intensity versus absorbance; η = Refractive index of the solvent; subscript x denotes the sample, and subscript ST

denotes the standard. Anthracene ($\Phi = 0.27$ in ethanol) was used as a standard in ethanol. The slit width was kept constant for both standard and samples. Absorbance was measured using a SHIMADZU UV-2450 spectrophotometer.

4.4. Preparation of PBPLP nanogel/RGD conjugate

Surface carboxylic acid groups of PBPLP nanogels readily reacted with the amino groups of peptide (cyclo(Arg-Gly-Asp-Phe-Lys(mpa)) (c(RGDFK))) by using N-(3-dimethylaminopropyl)-N-ethylcarbodiimde hydrochloride (EDC) after activated with sulfo-N-hydroxysuccinimide ester (sulfo-NHS). Typically, 20 mg (1.0×10-5 mol) of EDC and 20 mg (9.2×10-5 mol) of sulfo-NHS were added to 20 ml of MES (2-(N-morpholino)ethanesulphonic acid) buffer (0.1 M, 10 mL, pH 6.0) containing 40 mg of PBPLP nanoparticles. The mixture was stirred for 4 h and centrifuged for 20 min. The nanoparticle pellets were resuspended in 20 ml of c(RGDFK) containing aqueous solution. The reaction was stirred overnight followed by 2 cycles of washing with DI water and centrifugation. The process of conjugation was monitored by FTIR spectroscopy.

4.5. Drug loading and drug release study

Drug (DOX) loading in PBPLP nanogels was carried out by incubation. Briefly, the PBPLP nanogel suspension (5 mg/ml) was mixed with DOX solution (1 mg/ml) and incubated overnight to allow Dox absorption in the nanogels under gentle stirring. Then the mixture was centrifuged at 15,000 rpm for 20 min to remove free DOX. The loading efficiency and loading content of nanogels were determined by measuring the absorbance of DOX at 490 nm of the aqueous medium retrieve after centrifugation. Actual drug concentrations were calculated from the calibration curve prepared with the standard DOX solution.

For drug release studies, 10 ml of DOX-loaded nanogels were placed in a dialysis bag (MWCO: 2000 g/mol) and dialyzed against two different buffer solutions, 0.1 M acetic acid (pH 5.2) and 0.1 M phosphate buffer (pH 7.4) in a shaking water bath at 37 °C in the absence of light. At predetermined time points, 1 ml of release medium was assayed spectrophotometrically by measuring at an excitation wavelength of 490 nm and an emission wavelength of 590 nm. The data were reported as mean value of three independent studies with the reported standard deviation.

4.6. In-vitro cytotoxicity of PBPLP nanogels

Briefly, 100 μL of PC3 (human prostate cancer in the late disease stage) (5×104 cells/ml) in DMEM supplemental medium, 10% fetal bovine serum and 1% of penicillin/streptomycin (100 U/ml penicillin and 100 μg/ml streptomycin) were culture in a 96-well plate (Costar®, Corning Inc., Corning, NY) for 24 h at 37° C, 5% CO2. The culture medium was then removed and supplied with PBPLP nanogel solutions at different concentrations (0–1 mg/ml) in complete DMEM media. After 24 h of incubation, the medium was replaced by 100 μL of fresh media (FBS free) and 20 μL of MTS stock solution. The cultures were incubated for another 4 h. The percentage of relative cell survival to the control (cells exposed to regular culture media) was calculated.

4.7. Pharmacological activity of drug loaded PBPLP nanogel

The pharmacological activity of DOX-loaded nanogels was evaluated against prostrate cancer (PC3) cells using MTT assay. The cells were seeded on 96-well plate at 5×104 cells per well and then incubated overnight (37 C, 10% CO2). After 24 h incubation, media was replaced by 200 μL of various dilutions of DOX-loaded PBPLP (5, 25, and 50) μg/ml nanogels. MTT assay was performed at various time points (12, 24, and 48) h to understand the pharmacological effects of the drug loaded PBPLP nanogels. Drug free nanogels (50 μg/ml) and 10 μg/ml DOX solution were used as positive and negative controls respectively. The percentage of relative cell survival to control (cells exposed to regular culture media) was calculated.

Cellular uptake and pharmacological response of the DOX-loaded nanogels were visualized using fluorescence microscopy. Briefly, cells were cultured sterilized coverslips (12 mm) and placed in 24-well plate. Cells were incubated for 24 h and replaced with PBPLP nanogel, DOX-loaded nanogel, and DOX solutions. After 24 h of the treatment, the cells were rinsed using the ice-cold PBS buffer three times and fixed using a 4% paraformaldehyde solution for 10 min at room temperature. Then the cells were monitored by fluorescence microscopy.

Notes

The authors declare no competing financial interest.

Acknowledgment

This work was supported in part by a National Cancer Institute R01 award (CA182670, USA), and a National Heart, Lung, and Blood Institute award (HL118498, USA).

Appendix A. Supplementary data

Supplementary data related to this article can be found at http://dx.doi.org/10.1016/j.bioactmat.2017.03.001.

References

[1] W. Gao, J.C. Lai, S.W. Leung, Functional enhancement of chitosan and nanoparticles in cell culture, tissue engineering, and pharmaceutical applications, Front. Physiol. 3 (2012) 321.
[2] S.M. Janib, A.S. Moses, J.A. MacKay, Imaging and drug delivery using theranostic nanoparticles, Adv. drug Deliv. Rev. 62 (11) (2010) 1052–1063.
[3] J. Panyam, V. Labhasetwar, Biodegradable nanoparticles for drug and gene delivery to cells and tissue, Adv. drug Deliv. Rev. 55 (3) (2003) 329–347.
[4] K.C.R. Bahadur, P. Xu, Multicompartment intracellular self-expanding nanogel for targeted delivery of drug cocktail, Adv. Mater 24 (48) (2016) 6479–6483.
[5] Y. Sekine, et al., A hybrid hydrogel biomaterial by nanogel engineering: bottom-up design with nanogel and liposome building blocks to develop a multidrug delivery system, Adv. Healthc. Mater 1 (6) (2012) 722–728.
[6] T. Xing, et al., Synthesis of disulfide-cross-linked polypeptide nanogel conjugated with a near-infrared fluorescence probe for direct imaging of reduction-induced drug release, ACS Appl. Mater Interfaces 4 (10) (2012) 5662–5672.
[7] M. Takeo, et al., A polyion complex nanogel, J. Colloid Interface Sci. 390 (1) (2013) 78–84.
[8] M.H. Xiong, et al., Lipase-sensitive polymeric triple-layered nanogel for "on-demand" drug delivery, J. Am. Chem. Soc. 134 (9) (2012) 4355–4362.
[9] H. Takahashi, S. Sawada, K. Akiyoshi, Amphiphilic polysaccharide nanoballs: a new building block for nanogel biomedical engineering and artificial chaperones, ACS Nano 5 (1) (2010) 337–345.
[10] M. Gou, et al., Efficient inhibition of C-26 colon carcinoma by VSVMP gene delivered by biodegradable cationic nanogel derived from polyethyleneimine, ACS Nano 4 (10) (2010) 5573–5584.
[11] W. Park, S.J. Park, K. Na, Potential of self-organizing nanogel with acetylated chondroitin sulfate as an anti-cancer drug carrier, Colloids Surf. B Biointerfaces 79 (2) (2010) 501–508.
[12] E.B. Dickerson, et al., Chemosensitization of cancer cells by siRNA using targeted nanogel delivery, BMC Cancer 10 (2010) 10.
[13] A.M. Eckman, et al., Drug release patterns and cytotoxicity of PEG-poly (aspartate) block copolymer micelles in cancer cells, Pharm. Res. 29 (7) (2012) 1755–1767.
[14] W. Yang, et al., Fluorescent mannose-functionalized hyperbranched poly (amido amine) s: synthesis and interaction with E. coli, Biomacromolecules 11 (7) (2010) 1840–1846.
[15] Z. Yang, et al., Pharmacokinetics and biodistribution of near-infrared fluorescence polymeric nanoparticles, Nanotechnology 20 (16) (2009) 165101.
[16] S. Toita, et al., Protein-conjugated quantum dots effectively delivered into living cells by a cationic nanogel, J. Nanosci. Nanotechnol. 8 (5) (2008)

2279–2285.
[17] U. Hasegawa, et al., Nanogel-quantum dot hybrid nanoparticles for live cell imaging, Biochem. Biophys. Res. Commun. 331 (4) (2005) 917–921.
[18] W. Wu, et al., Chitosan-based responsive hybrid nanogels for integration of optical pH-sensing, tumor cell imaging and controlled drug delivery, Biomaterials 31 (32) (2010) 8371–8381.
[19] P. Anilkumar, et al., Crosslinked carbon dots as ultra-bright fluorescence probes, Small 9 (4) (2013) 545–551.
[20] L.A. Osminkina, et al., Photoluminescent biocompatible silicon nanoparticles for cancer theranostic applications, J. Biophot. 5 (7) (2012) 529–535.
[21] D. Wang, T. Imae, Fluorescence emission from dendrimers and its pH dependence, J. Am. Chem. Soc. 126 (41) (2004) 13204–13205.
[22] J. Yang, et al., Development of aliphatic biodegradable photoluminescent polymers, Proc. Natl. Acad. Sci. U. S. A. 106 (25) (2009) 10086–10091.
[23] R.T. Tran, J. Yang, G.A. Ameer, Citrate-based biomaterials and their applications in regenerative engineering, Annu. Rev. Mater. Res. 45 (2015) 277–310.
[24] Y. Zhang, et al., Fluorescence imaging enabled urethane-doped citrate-based biodegradable elastomers, Biomaterials 34 (16) (2013) 4048–4056.
[25] Z. Xie, et al., Development of intrinsically photoluminescent and photostable polylactones, Adv. Mater. 26 (26) (2014) 4491–4496.
[26] D. Gyawali, et al., Fluorescence imaging enabled biodegradable photostable polymeric micelles, Adv. Healthc. Mater. 3 (2) (2014) 182–186.
[27] J.P. Kim, et al., Citrate-based fluorescent materials for low-cost chloride sensing in the diagnosis of cystic fibrosis, Chem. Sci. 8 (1) (2017) 550–558.
[28] Z. Xie, et al., Synthesis and characterization of citrate-based fluorescent small molecules and biodegradable polymers, Acta Biomater. (2017), http://dx.doi.org/10.1016/j.actbio. 2017.01.019.
[29] A.M. Eckman, et al., Drug release patterns and cytotoxicity of PEG-poly(aspartate) block copolymer micelles in cancer cells, Pharm. Res. 29 (7) (2012) 1755–1767.